Quaternary Science Reviews 200 (2018) 395–405

Contents lists available at ScienceDirect

Quaternary Science Reviews

journal homepage: www.elsevier.com/locate/quascirev

Mt. Fuji Holocene eruption history reconstructed from proximal lake sediments and high-density radiocarbon dating

S.P. Obrochta [a, *], Y. Yokoyama [b], M. Yoshimoto [c], S. Yamamoto [c], Y. Miyairi [b], G. Nagano [b, 1], A. Nakamura [d], K. Tsunematsu [c, 2], L. Lamair [e], A. Hubert-Ferrari [e], B.C. Lougheed [f], A. Hokanishi [g], A. Yasuda [g], V.M.A. Heyvaert [h, i], M. De Batist [i], O. Fujiwara [d], the QuakeRecNankai Team[3]

[a] *Akita University Graduate School of International Resource Science, Japan*
[b] *University of Tokyo Atmosphere and Ocean Research Institute, Japan*
[c] *Yamanashi Prefectural Government Mount Fuji Research Institute, Japan*
[d] *Geological Survey of Japan, AIST, Japan*
[e] *University of Liège Department of Geography, Belgium*
[f] *Laboratoire des Sciences du Climat et de l'Environnement LSCE/IPSL, CNRS-CEA-UVSQ, Université Paris-Saclay, France*
[g] *University of Tokyo Earthquake Research Institute, Japan*
[h] *Geological Survey of Belgium, Royal Belgian Institute of Natural Sciences, Belgium*
[i] *Ghent University Department of Geology, Belgium*

A R T I C L E I N F O

Article history:
Received 3 June 2018
Received in revised form
29 August 2018
Accepted 1 September 2018
Available online 10 October 2018

A B S T R A C T

An 8000-year lacustrine sediment record from Lake Motosu (Fuji Five Lakes) records several eruptions, including potentially unreported events, of the active Mt. Fuji volcano, which receives approximately 47 million annual visitors. A high-fidelity age model is constructed from tephra ages and high-density radiocarbon dating of terrestrial macrofossil and bulk organic matter. Variability in lake reservoir age is constrained by modern lake water radiocarbon measurement and reverse calibration of tephra calendar ages. We present more accurate ages for known eruptions, detect a wider distribution of ejecta for several eruptions, including the most recent summit eruption, and potentially identify previously undetected flank eruptions. There are closely spaced scoria-fall layers that may be difficult to differentiate as separate events in land-based surveys. These results demonstrate the utility of lacustrine sediments as powerful tools for understanding characteristics of volcanic eruptions.

1. Introduction

The Japanese archipelago is distributed along a triple junction at the intersection of the North American, Pacific, and Philippine Sea Plates. The resulting tectonic activity formed Mt. Fuji, an active volcano adjacent to the Tokyo metropolitan area (Fig. 1). Based on data compiled by Shizuoka and Yamanashi Prefectures, the Mt. Fuji area attracted approximately 47 million visitors during 2015. Volcanic disaster mitigation plans for this region have been developed taking into account historical and geological information, the latter obtained through a number of primarily land-based geological field surveys (e.g., Yamamoto et al., 2005b; Ishizuka et al., 2007) and a small number of lake cores (Koshimizu et al., 2007) from the northwestern flank of Mt. Fuji. Regional stratigraphy is constrained by the presence of four volcanic marker beds, the Aira-Tn, Kikai-Akahoya, Amagi Kawagodaira, and Kozushima Tenjosan, that are derived from well-dated eruptions of distal volcanoes and, in contrast to the typically mafic composition of Mt. Fuji eruption products, comprised of felsic pumice (Fig. 2). The ages of prehistorical Mt. Fuji eruptions are based on radiocarbon dating of primarily charred material taken from within, above, or below volcanic deposits. However, the reported calendar ages are not always consistent with their observed stratigraphic order and position relative to Kawagodaira pumice-fall layer (Yamamoto et al.,

* Corresponding author.
E-mail address: obrochta@gipc.akita-u.ac.jp (S.P. Obrochta).

[1] Present address: Geospatial Information Authority of Japan, Ministry of Land, Infrastructure, Transport, and Tourism.
[2] Present address: Yamagata University, Faculty of Science, Japan.
[3] Members of the QuakeRecNankai Team: Boes, E., Brückner, H., De Rycker, K., Garrett, E., Ono, E., Riedesel, S., Sato, Y., Shishikura, M., and Walstra, J.

https://doi.org/10.1016/j.quascirev.2018.09.001
0277-3791/

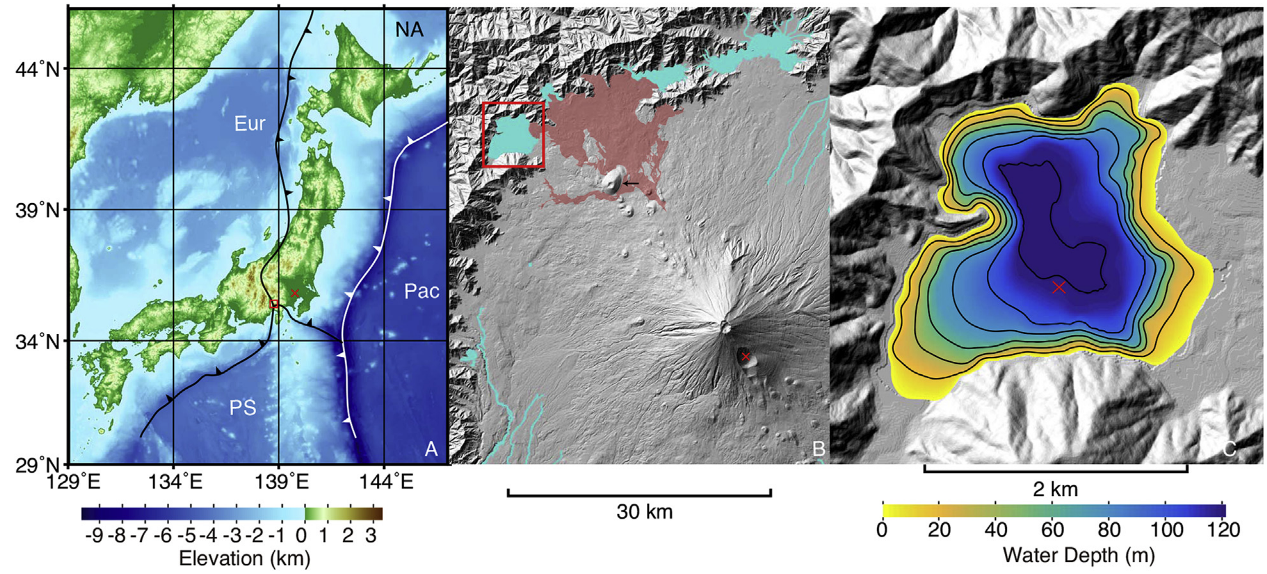

Fig. 1. A) Topographic map of Japan with bathymetery and plate boundaries (Eur: Eurasian; PS: Philippine Sea; NA: North American; Pac: Pacific). Red X indicates the location of Tokyo within the Kanto Plain, the surrounding area of low altitude and relief. Red square indicates region shown in panel B. B) Shaded elevation map of the Mt. Fuji region. Four of the Fuji Five lakes are shown. From West to East are Lake Motosu (indicated by with the box), Lake Shojiko, Lake Sai, and Lake Kawaguchi (See Fig. 10 for the location of Lake Yamanaka, the Easternmost lake.). The outcropping area of the Aokigahara lava flow is indicated by shading, the Omuro Crater (located between Lake Motosu and Mt. Fuji) is indicated by an arrow, and the Hoei Crater is indicated by an X. C) Lake Motosu shown with bathymetry survey data collected in 1964 by the Geospatial Information Authority of Japan. Contour interval is 20 m. Site MOT15-2 is denoted. (For interpretation of the references to color in this figure legend, the reader is referred to the Web version of this article.)

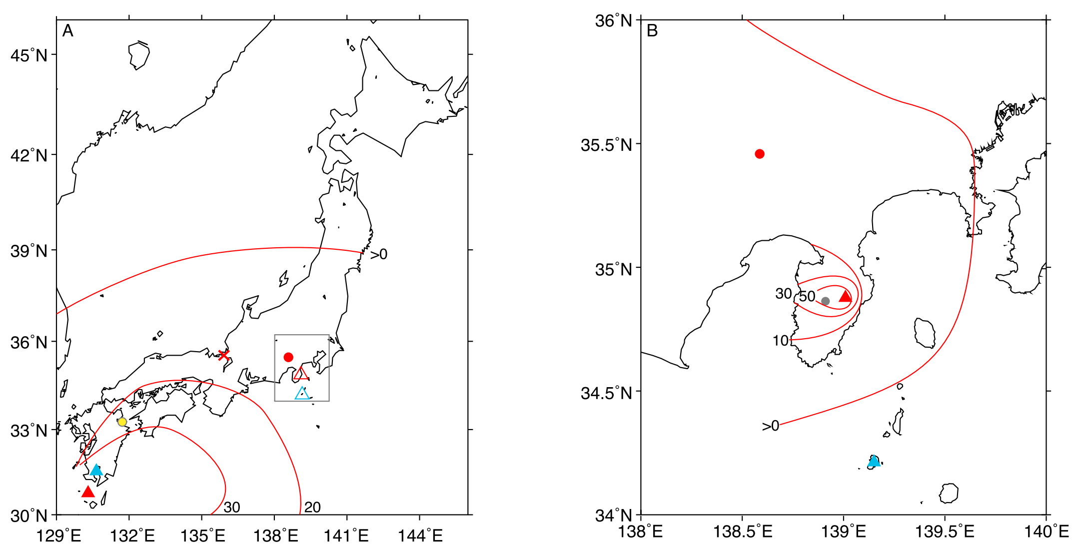

Fig. 2. Locations of four volcanoes that deposited pumice (widespread tephra) in the Lake Motosu region (red circle) during the Late Pleistocene. A) Isopach in centimeters of the Kikai Akahoya (K-Ah; red filled triangle) eruption at ~7 ka. The K-Ah proximal sample was obtained from Oita City, Oita Prefecture (33° 12.27′ N, 131° 40.64′ E; yellow circle). Also shown is the location of the Aira Caldera, which produced the AT tephra at ~30 ka (blue filled circle; distribution not shown). For reference, the location of Lake Suigetsu is indicated by the X. B) Isopach for the Izu-Amagi Kawagodaira (red filled triangle) eruption at ~ 3 ka. Sampling locations of the Kg pumice-fall layers (34° 54.07′ N, 138° 57.34′ E and 34° 52.63′ N, 138° 57.17′ E) and the pyroclastic density current (34° 54.84′ N, 138° 58.06′ E) are indicated by the gray circle. The Kozushima Tenjosan volcano (blue filled triangle) erupted in CE 838. Historical records suggested pumice from this eruption was distributed in the Mt. Fuji region but geological fieldwork is limited, with a thin layer reported from the southern flank (Sugihara et al., 2001). Tephra from all four volcanoes has been discovered in Lake Suigetsu (Smith et al., 2013, McLean et al., 2018). Isopach maps after Machida and Arai (2003). (For interpretation of the references to color in this figure legend, the reader is referred to the Web version of this article.)

2005b, Fig. 3). The current Mt. Fuji hazard map was created using the best information available at the time (Fuji Hazard Map Committee Members, 2004) and is slated for revision by 2020. Because eruption age and ejecta distribution are fundamental for hazard assessment, increased accuracy in reconstructing Mt. Fuji activity will contribute to improving the regional disaster mitigation plan with respect to eruption scenario and evacuation area.

Recent work has demonstrated the utility of lacustrine sediments in providing more accurate ages for volcanic depositions (e.g., Björck et al., 2006; Van Daele et al., 2014; McLean et al., 2018), particularly when high-density dating is performed (Blaauw et al., 2018). In 2014 and 2015, we carried out a coring campaign at four of the Fuji Five Lakes, Motosu, Sai, Kawaguchi, and Yamanaka. These are tectonically-controlled and distributed in an East-West trend along the Northern flank of the Mt. Fuji volcano. Given the prevailing Northwesterly wind, Lake Yamanaka, located on the Eastern

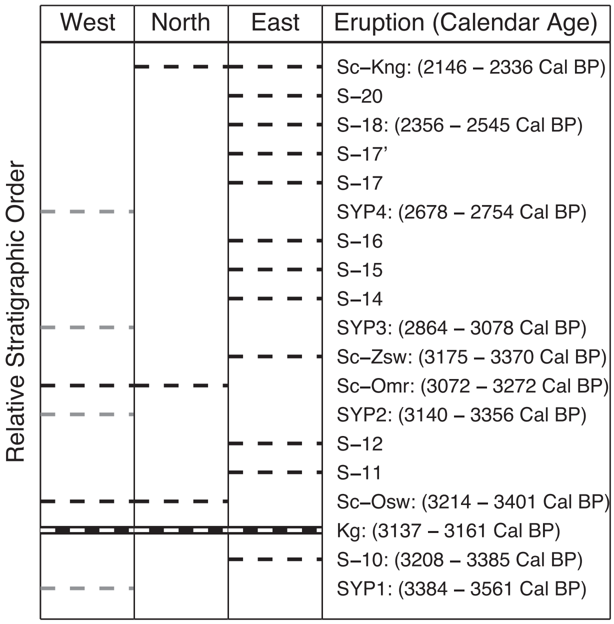

Fig. 3. Relative stratigraphic order of Mt. Fuji eruptions during the Subashiri-C Stage showing scoria-fall deposits (black lines), pyroclastic density currents (gray lines), and the Kawagodaira (Kg) widespread tephra (white and black dashed line). Age of the Kg eruption from Tani et al. (2013). Ages of Mt. Fuji eruptions are from Yamamoto et al. (2005a; 2005b) and are recalibrated here for consistency with calibrated radiocarbon dates from Lake Motosu using MatCal (Lougheed and Obrochta, 2016) with IntCal13 (Reimer et al., 2013).

flank of the volcano, is situated to record the largest number of eruptions. However, thick, coarse volcanic deposits, impenetrable with a piston corer, resulted in the recovery of only short gravity cores.

We therefore focus on a much longer, apparently continuous record recovered from Lake Motosu (Site MOT15-2) that is dated at centennial-resolution and contains five scoria-fall layers deposited over the past ~3000 years. Lake Motosu preserves records of paleoenvironmental change, seismic activity, and volcanic eruptions (e.g., Lamair et al., 2018), and with a Westerly relative position, upstream of the prevailing wind direction, it is positioned to record Western flank eruptions and several of the larger summit eruptions. To date, relatively few scoria-fall deposits have been identified along the Northwestern flank of the volcano (Yamamoto et al., 2005b). Thus, their presence would indicate a wider distribution than previously thought and allow us to better evaluate the discrepancy between their reported ages and observed stratigraphic order. The Lake Motosu record shows the potential for the Fuji Five Lakes to refine the chronology of Mt. Fuji eruptions, which could be furthered through rotary drilling of Lake Yamanaka.

2. Background

2.1. Regional marker beds

The four Late Pleistocene pumice marker beds deposited in the Mt. Fuji region are relatively widespread tephras that are not sourced from Mt. Fuji. The older two of these, the Aira-Tn (AT) and the Kikai-Akahoya (K-Ah) are derived from the Aira and Kikai Calderas on the southern tip of Kyushu, the southernmost of Japan's main islands (Fig. 2A). The younger two tephras are sourced from the Kawagodaira cone of the Amagi volcano and from the Tenjosan dome on the volcanic Kozushima island in the Izu arc, each South of Mt. Fuji. These two volcanoes produced the more regionally-dispersed Kawagodaira pumice (Kg) and the Kozushima-Tenjosan (Iz-Kt) tephra, respectively. All four of these tephras have been identified in Lake Suigetsu in central Japan (35° 35′ N, 135° 53′ E), 240 km from Lake Motosu; The At and K-Ah are deposited in Suigetsu as visible layers (Smith et al., 2013), while the Kg and Iz-Kt are cryptic (McLean et al., 2018).

The age of the AT eruption has been determined by radiocarbon dating on selected organic fractions of charred material retrieved from the pyroclastic density current, obtaining an age of 25,120 ± 270 ^{14}C yr BP (Miyairi et al., 2004), which calibrates to 28,585–29,871 cal BP (2σ) using IntCal13 (Reimer et al., 2013) and MatCal (Lougheed and Obrochta, 2016). The SG06 Suigetsu varve chronology (Nakagawa et al., 2012) suggests a slightly older age range for the AT eruption (29,820–30,198 cal BP) and an age of 7165–7303 cal BP for the K-Ah eruption (Smith et al., 2013). The age of the Kg eruption has been determined precisely through ^{14}C wiggle matching (3149 ± 12 Cal BP; Tani et al., 2013), and the Iz-Kt is a historical eruption that occurred in 838 CE (e.g., Sugihara et al., 2001).

The Kg and K-Ah tephras are the most relevant for this study (Fig. 2). The AT tephra predates the maximum age of our record. The dispersal pattern of the Iz-Kt is not well established from field studies (Machida and Arai, 2003), but historical records suggest it was deposited in the Mt. Fuji region, and it has been reported to be ~1 mm thick at a distance of 120 km from the source volcano (Sugihara et al., 2001). Discovery of the Iz-Kt tephra in Lake Suigetsu (McLean et al., 2018) suggests it is present in Lake Motosu, though likely as a non-visible cryptotephra.

2.2. Mt. Fuji development

Two distinct classification schemes using the stratigraphy of lava flows (Tsuya, 1968) and tephra deposits (Machida, 1977) have been proposed to describe the development of Mt. Fuji. Takada et al. (2016) recently reconciled these two schemes and classify the development of Mt. Fuji into three stages over the past 100 ka, the Hoshiyama, the Fujinomiya, and the Subashiri.

The Hoshiyama Stage, previously referred to as the Ko- (older) Fuji (Tsuya, 1968), lasted from 100 ka to ~17 ka during which explosive eruptions widely distributed large amounts of basaltic tephra over the Kanto Plain. Tsuya (1968) grouped the subsequent two stages, the Fujinomiya and the Subashiri, into the Shin- (younger) Fuji Volcano. During the Fujinomiya Stage, lasting from 17 ka to 8 ka, volcanic activity was dominated by large-volume lava flows extending up to 40 km from the summit. The current Subashiri Stage, beginning from 8 ka, is subdivided based on differences in eruption style. The Subashiri-A Stage (8–5.6 ka) was marked by reduced activity, with mainly sporadic, modest eruptions. The modern volcanic cone was emplaced during the Subashiri-B Stage (5.6–3.5 ka) as eruptions became more frequent. The Subashiri-C Stage (3.5–2.3 ka) saw explosive basaltic Plinian and sub-Plinian summit eruptions, as well as explosive flank eruptions. Of the over 14 scoria-fall deposits that have been registered in total during this Stage (Miyaji, 1988), only two are detected in the Lake Motosu area (Northwestern flank; Fig. 3). Four pyroclastic density currents (PDCs) flowed down the western flank. These include the first two of the “Shin-Fuji Younger” PDCs (SYP1 and 2) with reported ages (Yamamoto et al., 2005b) of 3384–3561 and 3140–3356 cal BP, between which the Osawa Scoria (Sc-Osw) was deposited (3214–3401 cal BP). An eruption on the northwest flank then created the Omuro scoria-fall deposit (Sc-Omr; 3072–3272 cal BP); it was followed by the deposition of SPY3 and SPY4 (2864–3078 and 2678–2754 cal BP). The last known summit eruption (Kengamine; Sc-Kng) occurred at the end of the Subashiri-C, with subsequent eruptions limited to flank volcanoes during the Subashiri-D Stage (2.3 ka - present). Two large historic Mt. Fuji

Table 1
Sediment core coordinates and recovery depths.

Core	Lat	min	lon	min	top (m)	length (cm)	location
MOT15-2B-G-1	35	27.69	138	35.156	0	32	Japan
MOT15-2A-G-1	35	27.69	138	35.156	0	27	Belgium
MOT15-2D-H-1	35	27.684	138	35.155	0	184	Japan
MOT15-2A-H-1	35	27.683	138	35.154	0	185	Belgium
MOT15-2E-H-1	35	27.686	138	35.159	1	189	Japan
MOT15-2C-H-1	35	27.683	138	35.156	1	187	Belgium
MOT15-2B-H-1	35	27.684	138	35.154	2	157	Split (Japan/Belgium)

eruptions have occurred. The AD 864–866 Jogan eruption resulted in the Aokigahara Lava flow extending into Lake Motosu. In AD 1707, the Hoei eruption occurred on the southeastern flank.

2.3. Lake Motosu

Lake Motosu (35° 27.833′ N, 138° 35.167′ E; 900 m asl; Fig. 1) is situated directly proximal to the Mt. Fuji volcano and is the deepest of the Fuji Five Lakes. The last bathymetric survey was conducted in 1964, during which time the maximum depth and basin size were reported to be 121.6 m and 4.7 km^2, respectively (Geospatial Information Authority of Japan, 2018). The AT tephra was identified in a deep borehole along the eastern shore of the lake at a depth of 172 m overlying lake sediments, indicating Lake Motosu has existed since at least ~30 ka (Koshimizu et al., 2007).

Hamada et al. (2012) performed 18 monthly hydrographic surveys between May 2009 and October 2010, sampling between a depth of 110 m and the surface. During this time, the lake was stratified except during February and March. Hamada et al. (2012) also estimated the catchment size to be between 24.64 and 9.81 km^2 and calculated water balance, reporting ~1500 mm/y and between ~200 and ~475 mm/y of water input by direct rainfall and groundwater percolation, respectively. This was balanced by evaporation of ~600 mm/y, removal of ~530 mm/y for hydroelectric power generation, and groundwater outflow of between ~560 and 850 mm/y. There is no year-round, sustained river input.

3. Methods

3.1. Coring and stratigraphic correlation

Two gravity and seven hammer-piston sediment cores were recovered from Lake Motosu in November 2015 using an Uwitec platform (Table 1; Fig. 4). Two-meter piston cores were recovered at overlapping depths below the lake floor (e.g., 0–2 m, 1–3 m, 2–4 m) by adding extensions to the core barrel. Duplicate cores were retrieved to a depth of 3 m, with one set of cores being transported to Belgium where they were split for parallel analyses. The piston core from 2 to 4 m was not duplicated and split in the field. One half was transported to Belgium. Cores remaining in Japan were split at the Yamanashi Prefecture Mount Fuji Research Institute and immediately imaged and described.

Color reflectance (i.e., L*, a*, b*) was calculated from the core images (e.g., Obrochta et al., 2014). Cores in Japan were analyzed by X-Ray fluorescence (XRF) at the Kochi Core Center using an ITRAX XRF scanner set to 30 kV with a 1 cm step and a Hitachi Pratico CT Scanner, respectively. XRF data from cores transported to Belgium were collected with an Aavatech Core Scanner III at the MARUM, University of Bremen with a 2-mm step over a 1.2 cm^2 area and a down-core slit size of 2 mm at 30 kV. A composite, spliced section for the Japanese cores was constructed through visual stratigraphic correlation, aided by the XRF and color reflectance data, to create a continuous record to 3.67 m composite depth (mcd; Table 2). The depth scales of the Belgian cores were then reprojected to precisely align them to the Japanese composite splice.

3.2. Widespread tephra analysis

Two visible, rhyolitic pumice layers (not of Mt. Fuji origin) at 1.915 mcd (5–10 mm thick; MOT15-2D-H1 186 cm) and 3.455 mcd (~5 mm thick; MOT15-2B-H1 135 cm) are present. Based on reported tephra thickness, distribution, and age, these are likely to be the Kg (3149 ± 12 cal BP; Tani et al., 2013) and K-Ah (7234 ± 69 cal BP; Smith et al., 2013) tephras. To confirm this, geochemical

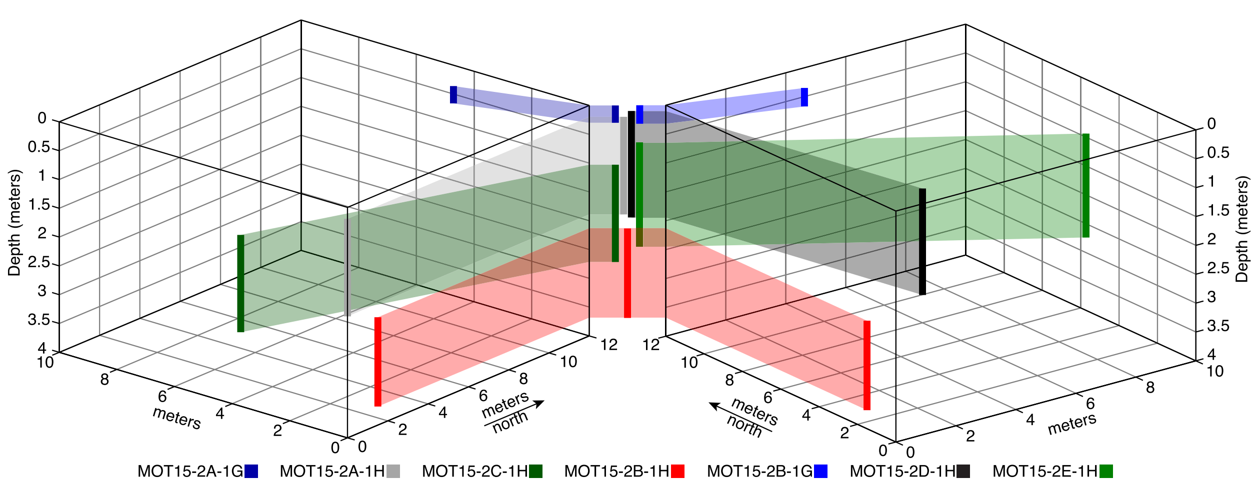

Fig. 4. 3D distribution of sediment cores recovered from Lake Motosu. The left panel shows cores archived in Belgium, and the right panel those archived in Japan. Both sets of axes are centered on the same geographic coordinates. Visual stratrigraphy and XRF data were used to align the cores archived in Belgium to the Japanese cores.

Table 2
Composite splice table.

Core	Interval (cm)	tie type	Core	Interval (cm)	Length (cm)	Depth (mcd)
		start	MOT15-2B-1G	15		0
MOT15-2B-1G	35	tie to	MOT15-2D-1H	14.5	20	0.2
MOT15-2D-1H	187	tie to	MOT15-2E-1H	129	172.5	1.925
MOT15-2E-1H	182	tie to	MOT15-2B-1H	35	53	2.455
MOT15-2B-1H	159	end			124	3.695

analysis of 10 glass shards from each tephra was performed by electron probe microanalysis (EPMA) at Earthquake Research Institute (University of Tokyo). A JEOL-8800 microprobe was used with a15 KeV potential, 12 nA current, and 10 μm beam width for 40 s (e.g., Suzuki et al., 2013). Columbia River Basalt (USGS BCR-2) was used as a secondary standard. Measured components are Na_2O, MgO, SiO_2, P_2O_5, SO_3, Cl, Al_2O_3, K_2O, CaO, FeO, TiO_2, and V_2O_3. Shards collected proximal to each volcano were also analyzed for comparison to the unknown tephras in the sediment cores. The Kg pyroclastic density current was sampled (34° 54.84′ N, 138° 58.06′ E), and the Kg pumice-fall layer was sampled at two locations (34° 54.07′ N, 138° 57.34′ E and 34° 52.63′ N, 138° 57.17′ E). The K-Ah tephra was sampled from Oita City, Oita Prefecture (33° 12.27′ N, 131° 40.64′ E; Fujiwara et al., 2010).

3.3. Chronology

3.3.1. Radiocarbon analyses

Radiocarbon analyses of terrestrial macrofossils, bulk organic matter, and modern lake water were performed at the Atmosphere and Ocean Research Institute, The University of Tokyo, using a single stage accelerator mass spectrometer (AMS) following the procedures described in Yamane et al. (2014) and Yokoyama et al. (2016). Lake water samples were immediately spiked with $HgCl_2$. Radiocarbon ages were calibrated using MatCal (Lougheed and Obrochta, 2016) and the IntCal13 calibration curve (Reimer et al., 2013). Bulk samples were corrected for reservoir effect (due to the contribution of relatively older carbon) as described in the next section. For a portion of the bulk radiocarbon dates, C/N data was obtained during the radiocarbon analyses.

3.3.2. Bulk organic matter radiocarbon correction

To investigate the influence of older carbon upon bulk radiocarbon dates (the so-called reservoir effect), bulk organic matter ^{14}C dates were performed at depths coinciding with the depths (1.915 mcd and 3.455 mcd) of the two widespread tephras of known calendar age. The calendar ages of the tephras were reverse calibrated into an expected ^{14}C age probability density function (PDF) according to the IntCal13 (Reimer et al., 2013) calibration curve using the methodology described in Lougheed et al. (2017). The reservoir effect offset was calculated as the difference between the actual median ^{14}C ages according to the reverse calibration process. Uncertainty was calculated as the difference in the continuous 1σ ranges of the radiocarbon year PDFs. The root sum of squared uncertainty for the analytical age and the offset was calculated and applied to each bulk date prior to calibration. For bulk dates between 1.915 mcd and 3.455, reservoir age and uncertainty was linearly interpolated. Along with the age of the modern lake water, this provides three points for assessing the old carbon-induced reservoir effect for bulk ^{14}C dates.

3.3.3. Age modeling

Age modeling was performed in a deterministic 10^5 iteration Monte Carlo routine, called “undatable”, that considers depth uncertainty and was adapted from Obrochta et al. (2017). The model was further modified in Webster et al. (2018) to include Gaussian accumulation rate uncertainty between adjacent dates by adding intermediate points in between age-depth points. Anchoring is also included to prevent the modeled median from drifting away from the region of highest probability of the upper- and lower-most dates, which is a consequence of including depth uncertainty. Material for bulk dates was subsampled from 2-cm samples, but the precise sample depth is uncertain because only a small amount of sediment was needed for dating. An initial 2000-iteration run was performed by the same method as the primary simulation (described below) to obtain the top and bottom anchor points. These are extrapolated points based on the median age and depth of the upper- and lower-most two dates.

Bulk dates from the same levels as the tephras were excluded for a total of 31 dates used in the model. The modeling strategy uses the relatively precise macrofossil ($n = 5$) and tephra ages ($n = 2$) to anchor the less-well constrained bulk dates ($n = 24$) by bootstrapping the bulk dates, retaining ~50% of all data for each iteration (i.e., 15 dates, always including each macrofossil and tephra). For each iteration, age-depth modeling was performed in an upwards direction from the stratigraphically lowest date by selecting one probability-weighted age from the 95.4% (2σ) age range of each calendar age PDF and, in the case of bulk dates, one randomly sampled depth from the uniformly-distributed depth PDF. Dates producing age reversals are automatically skipped (i.e. regarded as an outlier) in an iteration if resampling of the PDF does not clear the reversal.

Results of the modeling are stored in a 63×2 x n matrix, where the first dimension corresponds to the number of dates (31), plus the additional points for added accumulation rate uncertainty between dates (30) and the two anchors. The second dimension holds the sampled age and depth, and n is the number of simulations. After all simulations were completed, the anchors were discarded and the median depth and age were calculated. Finally, results were interpolated to a 1-cm resolution and a probability density cloud was created by looping through the modeled ages to calculate the 1st through 99th percentiles. Model details and performance are discussed in Lougheed and Obrochta (submitted).

4. Results

4.1. Sediment character

Sediments at Site MOT15-2 are characterized by a mixture of siliceous biogenic and fine clastic particles punctuated by coarser dark layers rich in scoria with increased Ca, Sr, and Ti content relative to background sediment. Lake Motosu is virtually devoid of $CaCO_3$ sediments. Scoria grains were subsampled from split cores and observed with a reflected light microscope to determine grain morphology and if coatings are present. These detailed observations of the scoria layers indicate that five are comprised of angular,

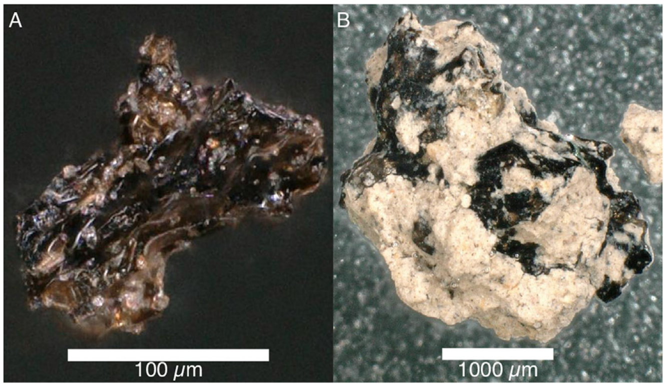

Fig. 5. A) photomicrograph of a clean, non-rounded scoria grain interpreted as being deposited by air-fall from MOT15-2E-1H (116 cm, ~1.84 mcd). Scale bar is 100 μm. B) A scoria grain coated with fine sediment that is interpreted to have been reworked (MOT15-2B-1H; 118 cm, ~3.26 mcd). Scale bar is 1 mm.

clean scoria (Fig. 5A) that are interpreted to have been deposited by air-fall. The other scoria layers appear reworked and contain 1) rounded grains suggesting transportation, 2) fine sediment embedded in vesicles, and 3) presence of vegetation and terrigenous material (Fig. 5B; e.g., Bertrand et al., 2014). The fall-deposits are preserved in Core MOT15-2D-1H, used in the composite splice, as well as in the off-splice interval of MOT15-2E-1H. 1-cm and ~0.75-cm thick fall-deposits occurs at 1.84 and 1.75 mcd. There is a ~5-cm layer of reworked material directly overlying the 1.75-mcd fall-deposit. Two mm-scale distinct fall-deposits appear at 1.44 and 1.43 mcd, followed a ~1-cm reworked scoria layer. The uppermost scoria fall-deposit is a ~0.5-cm scoria at 1.34 mcd.

4.2. Tephra analysis

The chemical composition of glass shards from the 1.915 mcd and 3.455 mcd tephras is indistinguishable from the shards sampled proximal to each volcano for the Kg and K-Ah eruptions, respectively (Fig. 6; See Supplemental online material). Relative to Smith et al. (2013), our data show slightly elevated silica content, perhaps indicating some loss of sodium, though silica content is similar to that of Machida and Arai (2003). This is likely due to difference in beam currents for analyses performed in Japan. The positive identification of the Kg and K-Ah tephras in these cores is consistent with the reported ages of the eruptions, as well as with the known distribution of ejecta.

4.3. Chronology

The radiocarbon age of the lake surface water is 222 ± 70 ^{14}C years. Bulk, uncalibrated radiocarbon dates are consistently offset from terrestrial macrofossils and reverse-calibrated tephras (Fig. 7A; Table 3). Correction using the measured age of the lake water results in good agreement to a depth of ~2 mcd, at which additional offset is detected between the Kg tephra and the corresponding bulk date (Fig. 7B). Similar offset is observed between the K-Ah tephra age and the bulk date from the same depth. At the levels of the Kg and K-Ah tephras, bulk dates are offset by an additional 414 ± 66 and 503 ± 118 years (Fig. 8A and B). This is added to the 222 ± 70 years measured from the modern lake water to obtain a down-core correction for all bulk dates (Fig. 8C). The C/N data obtained during AMS measurements show generally low values (~9), indicative of primarily aquatic organic matter (Fig. 8D). Thus, this offset is interpreted to primarily result from a reservoir age within the lake. After reservoir correction of all bulk dates,

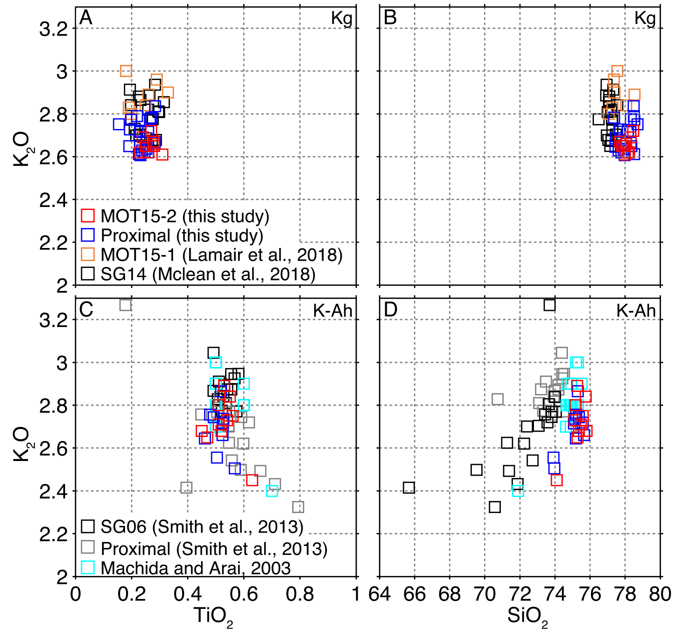

Fig. 6. Geochemistry of glass shards from MOT15-2 (red, this study). A and B) K_2O versus TiO_2 and K_2O versus SiO_2 for the 1.915-mcd pumice compared to data from shards collected proximal to the Kawagodaira (Kg) caldera (blue, this study), shards from Site MOT15-1 (orange, Lamair et al., 2018), and from Lake Suigetsu (black, McLean et al., 2018). C and D) The same for the 3.455-mcd pumice (red, this study) compared to proximal shards from the Kikai-Akahoya (K-Ah) eruption (blue, this study; gray, Smith et al., 2013; cyan, Machida and Arai, 2003) and distal shards subsampled from Lake Suigetsu sediment cores (black, Smith et al., 2013). Results indicate that these two pumices are from the Kg and K-Ah eruptions, which are well-constrained in age. Colors and axes ranges are consistent across all four panels. (For interpretation of the references to color in this figure legend, the reader is referred to the Web version of this article.)

there is good agreement between all bulk dates and tephras, except around 2.5 mcd where bulk dates are anomalously old (Fig. 8E). Age increases linearly with depth until a depth of ~3 mcd, at which sedimentation rate appears to decrease.

Age modeling results (Fig. 9) in an age of 380 cal BP (118–692 2σ) at 0.01 mcd, the depth of the uppermost radiocarbon date yr BP. An age of 8172 cal BP (8375–9060 2σ) is obtained at 3.615 mcd, the depth of the lowermost date. The age model produces mean and maximum sediment accumulation rates of ~55 and ~105 cm/ky, with a minima <10 cm/ky at the bottom of the spliced section. The modeled mean excludes the reversing age just below 2.5 mcd, with asymmetrical uncertainty skewed to older dates in this interval and at the sedimentation rate inflection point.

5. Discussion

Combining high-density dating, with an average of approximately one age control point per 10 cm, down-core reservoir age assessment, and a newly developed age model with improved treatment of uncertainty, we obtain a high-fidelity chronology for Site MOT15-2. This allows us to determine robust age ranges for the five scoria-fall layers deposited in apparently continuously accumulating background sediment during the Subashiri-C Stage. Previous work reconstructing volcanic history from lacustrine sediments was aided by the presence of annual laminations (Van Daele et al., 2014; Smith et al., 2013). However, we find that in the absence of varves, the needed chronological control may be obtained through multiple radiocarbon dates (e.g., Blaauw et al., 2011, 2018), particularly when augmented with terrestrial

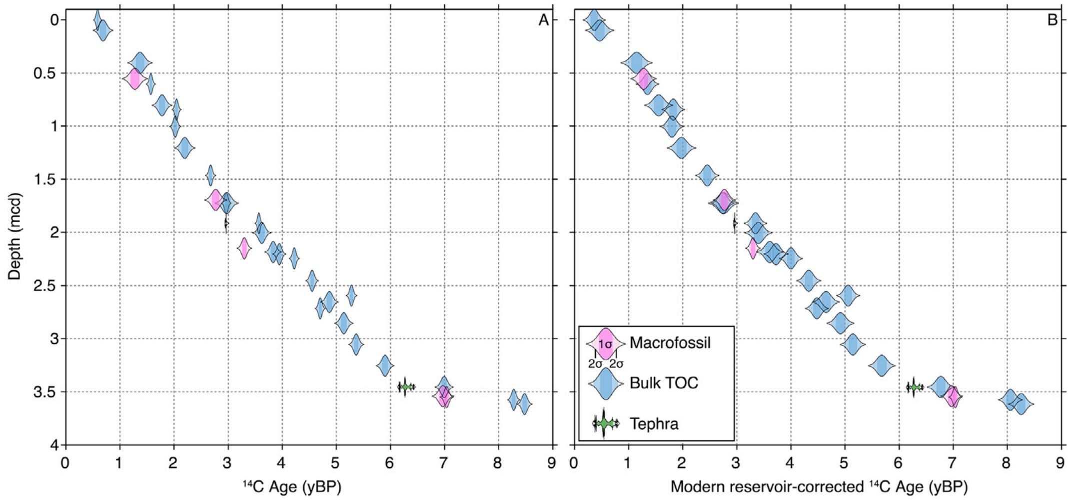

Fig. 7. Bulk (blue) radiocarbon, terrestrial macrofossil (red) radiocarbon, and reserve-calibrated tephra (green) ^{14}C age probability density functions. Dark and light regions denote the 1σ and 2σ ranges, respectively. A) Uncorrected bulk radiocarbon ages are offset from and older than terrestrial macrofossils. B) After correction by subtraction of the 222 ± 70-year reservoir age obtained by measuring the radiocarbon age of modern lake water, bulk dates are generally inline with terrestrial macrofossils to a depth of ~2 mcd, below which offset increases. Bulk dates nearby terrestrial macrofossils and from the same levels as the Kg and K-Ah tephras remain anomalously old. (For interpretation of the references to color in this figure legend, the reader is referred to the Web version of this article.)

Table 3
Radiocarbon dating for Site MOT15-2.

Lab ID	top (mcd)	bot (mcd)	14C age	14C err	C/N	Cal curve	R(t)	R(t) err	Median (cal BP)	95.4% HPD intervals	95.4% HPD intervals
YAUT-033229	0	0.02	587	25	9.16	intcal13	222	70	406	527-289 (0.955)	
YAUT-027014	0.09	0.11	688	65	10.44	intcal13	222	70	495	650-581 (0.15)	569-309 (0.804)
YAUT-027216	0.395	0.415	1370	82		intcal13	222	70	1077	1292-905 (0.937)	856-830 (0.015)
YAUT-027209	0.555	0.555	1277	87		intcal13	0	0	1195	1338-1047 (0.908)	1033-985 (0.047)
YAUT-027306	0.595	0.615	1571	28	12.27	intcal13	222	70	1268	1393-1171 (0.872)	1162-1077 (0.083)
YAUT-027224	0.795	0.815	1778	65		intcal13	222	70	1459	1692-1666 (0.02)	1628-1294 (0.934)
YAUT-033231	0.835	0.855	2047	28	9.74	intcal13	222	70	1755	1899-1566 (0.947)	
YAUT-027309	0.995	1.015	2023	36	11.47	intcal13	222	70	1727	1894-1552 (0.955)	
YAUT-027217	1.195	1.215	2199	68		intcal13	222	70	1935	2297-2263 (0.015)	2157-1699 (0.939)
YAUT-027311	1.455	1.475	2676	31		intcal13	222	70	2539	2725-2353 (0.955)	
YAUT-027212	1.695	1.695	2770	73		intcal13	0	0	2879	3059-3046 (0.015)	3044-2754 (0.941)
YAUT-027016	1.715	1.735	2975	78		intcal13	222	70	2880	3180-2711 (0.952)	
YAUT-027312	1.715	1.735	2965	30		intcal13	222	70	2854	3035-3011 (0.018)	3008-2744 (0.933)
YAUT-034928	1.91	1.92	3567	23		intcal13	636	94	3085	3351-2856 (0.955)	
YAUT-027017	1.995	2.015	3622	59	11.01	intcal13	641	97	3148	3402-2861 (0.949)	
YAUT-026935	2.15	2.15	3299	46		intcal13	0	0	3525	3637-3445 (0.932)	3426-3407 (0.023)
YAUT-027633	2.175	2.195	3832	52	9.56	intcal13	652	102	3398	3687-3662 (0.012)	3646-3137 (0.925)
YAUT-027532	2.195	2.215	3946	41		intcal13	653	102	3532	3830-3329 (0.936)	3291-3256 (0.019)
YAUT-033232	2.235	2.255	4222	31	9.91	intcal13	655	103	3867	4152-3585 (0.955)	
YAUT-027437	2.445	2.465	4552	40	9.20	intcal13	667	109	4306	4789-4763 (0.01)	4627-3971 (0.941)
YAUT-033233	2.585	2.605	5280	33	9.46	intcal13	675	113	5295	5589-4961 (0.954)	
YAUT-027438	2.645	2.665	4871	58	9.58	intcal13	679	115	4714	5062-4408 (0.936)	
YAUT-033236	2.705	2.725	4702	32	9.10	intcal13	682	116	4511	4835-4225 (0.931)	4203-4176 (0.016)
YAUT-027439	2.845	2.865	5138	60	9.43	intcal13	690	120	5095	5471-4815 (0.942)	
YAUT-027502	3.045	3.065	5367	48	8.88	intcal13	702	126	5373	5657-4966 (0.955)	
YAUT-027503	3.245	3.265	5901	58	9.42	intcal13	713	131	5959	6276-6226 (0.039)	6224-5657 (0.915)
YAUT-027504	3.445	3.465	6993	58	8.50	intcal13	725	137	7166	7441-6796 (0.953)	
YAUT-027206	3.54	3.54	6970	72		intcal13	0	0	7803	7940-7675 (0.955)	
YAUT-029402	3.545	3.555	7039	41		intcal13	0	0	7879	7956-7790 (0.955)	
YAUT-033237	3.565	3.585	8279	39		intcal13	725	137	8358	8609-8033 (0.949)	
YAUT-027516	3.605	3.625	8479	48		intcal13	725	137	8579	9000-8325 (0.955)	

macrofossils and tephra ages.

Although ejecta from three Subshiri-C Mt. Fuji eruptions, the Kengamine, Omuro, and Osawa (Fig. 3), is deposited along the northwestern side of the volcano, previous work (Miyaji, 1988) suggests erupted material is not distributed over Lake Motosu (Fig. 10). However, Lamair et al. (2018) geochemically analyzed scoria deposited in Lake Motosu and interpreted that it is sourced from Mt. Fuji. Nearby Lake Motosu, the only known volcanoes producing basaltic eruptions over the past 4000 years are Mt. Fuji, Izu-Oshima, and Miyake-Jima, but eruption products from the latter two volcanoes has not been observed in the Mt. Fuji region (Machida and Arai, 2003). We therefore interpret that Lake Motosu records five Mt. Fuji eruptions at median ages and 2σ ranges of 3042 (2858−3119 cal BP), 2930 (2798−3072 cal BP), 2458 (2165−2676 cal BP), 2438 (2145−2658 cal BP), and 2309 (2033−2572 cal BP; Table 4; Fig. 11).

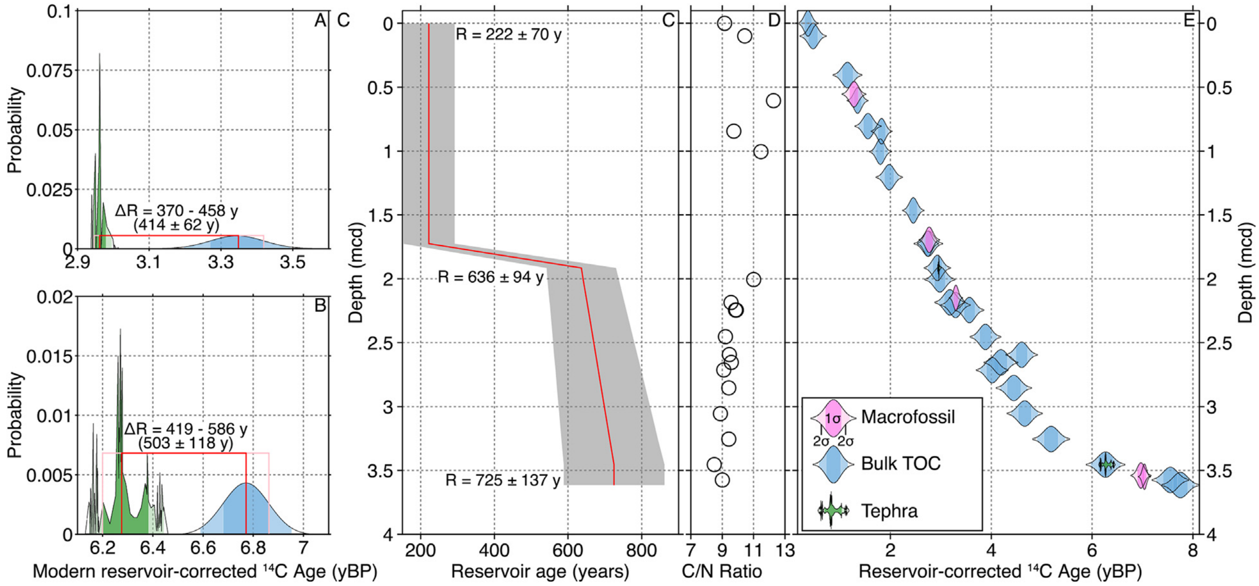

Fig. 8. Calculation of down-core changes in reservoir age using bulk dates corresponding to tephra layers. Difference in median ages and continuous 1σ ranges between bulk dates at the same depth as the Kg (A) and K-Ah tephras (B) suggest ΔR of 414 ± 62 years at 1.915 mcd and 503 ± 118 years at 3.455 mcd, respectively. C) The modern 222 ± 70-year reservoir age increases to 636 ± 94 at 1.915 mcd. Reservoir age and error is linearly increased in the interval between the Kg and K-Ah tephras to a maximum of 725 ± 137 at 3.455 mcd. D) C/N ratios are relatively low and vary little, suggesting a primarily aquatic source of organic matter and that the increase in bulk radiocarbon age is likely not due to increased input of old catchment soil but instead due to increased reservoir age. E) Uncalibrated, reservoir-corrected radiocarbon dates after application of reservoir age calculated from paired tephras and bulk dates. Bulk dates are inline with terrestrial macrofossils and tephras, with a generally linear sedimentation rate. Sedimentation rate decreases between the date at 3.245 mcd (YAUT-027503) and the K-Ah tephra. Except for a ~20-cm interval below 2.5 mcd, all dates are in stratigraphic order.

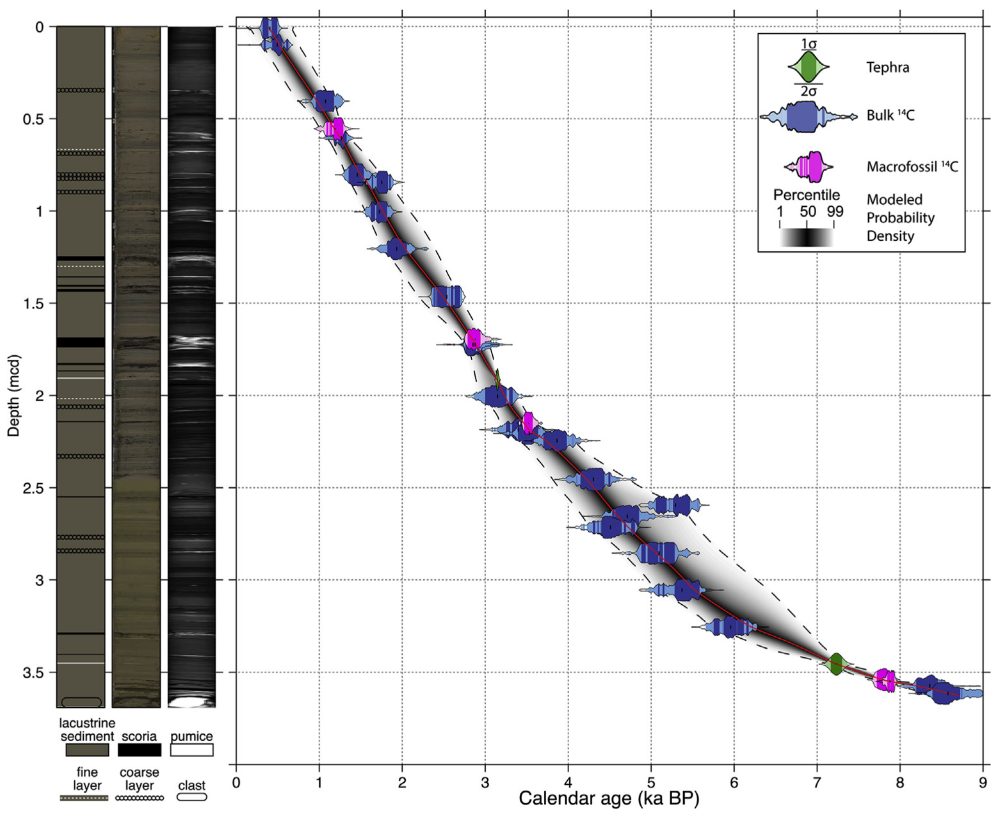

Fig. 9. Site MOT15-2 age model with (from left to right) generalized stratigraphic column, composite core image, and CT scan. The stratigraphic column shows the positions of scoria and pumice, as well as coarse and fine layers. Dark and light shading in calendar age PDFs indicates the calibrated 1σ and 2σ ranges, respectively. The modeled median age and 2σ range are indicated by the red solid and black dashed lines, receptively. The shaded density cloud reflects the 1 to 99th percentile range. Except for the two bulk dates paired with the Kg and K-Ah tephras (Fig. 8A and B), all radiocarbon dates are used in the age model, including the outlier at ~2.5 mcd (YAUT-033233). Uncertainty increases transiently above 3.5 mcd due to the inflection point in sedimentation rate and the presence of the outlier. (For interpretation of the references to color in this figure legend, the reader is referred to the Web version of this article.)

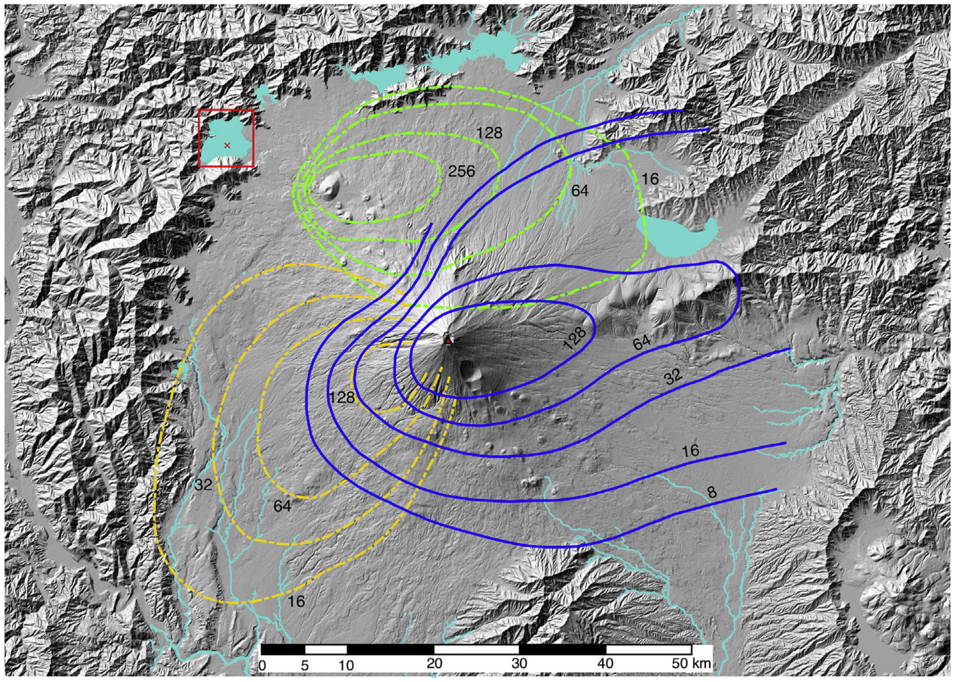

Fig. 10. Distribution and thickness (in centimeters), as determined by trench surveys, of the Osawa (Sc-Osw, yellow dashed line distributed to the Southwest), the Omuro (Sc-Omr, green dashed line), and the Kengamine (Sc-Kng, blue solid line) scoria deposits. These are the only Subashiri-C Stage larger eruptions previously noted to have distributed scoria on the northwestern flank of the volcano and, therefore, the most likely to be deposited at Lake Motosu. Distributions from Miyaji (1988). Lake Motosu and Site MOT15-2 are indicated by the box and X respectively. (For interpretation of the references to color in this figure legend, the reader is referred to the Web version of this article.)

Table 4
Revised ages of eruptions registered in Lake Motosu.

Eurption	Symbol	Modeled Median Age (cal BP)	Modeled 1σ	Modeled 2σ
Kengamine	Sc-Kng	2309	2174–2452	2033-2572
Unknown 2	Unk2	2438	2309–2569	2145–2658
Unknown 1	Unk1	2458	2331–2590	2165–2676
Omuro	Sc-Omr	2930	2859-3003	2798–3072
Osawa	Sc-Osw	3042	2965-3085	2858–3119

It is not possible to geochemically identify most individual Mt. Fuji eruptions due to extremely low variability in chemical composition (e.g., Ishizuka et al., 2007). Therefore, we consider the age of each scoria deposit relative to previously published ages (Yamamoto et al., 2005b), reported distribution (Fig. 10), and stratigraphic position relative to the Kg tephra (Fig. 3). Each scoria-fall layer deposited at Site MOT15-2 is above the Kg tephra, ruling out the eruptions generating the SYP1 pyroclastic density current and the S-10 scoria.

The oldest scoria-fall layer recovered at MOT15-2 corresponds to the Osawa eruption (Fig. 11). The Osawa directly overlies the Kg tephra, and there are no Mt. Fuji eruptions reported in between. This is consistent with the stratigraphic order preserved at Lake Motosu. Above the Osawa, the next eruption to result in scoria-fall on the northwestern flank was the Omuro. The ages of these two eruptions, originally obtained by dating charred material (Yamamoto et al., 2005b), are recalibrated here for consistency, obtaining 2σ age ranges of 3214–3401 and 3072–3272 cal BP, respectively (Fig. 3). The 2σ age ranges for these two eruptions are derived from calibrated ^{14}C ages, which only include ^{14}C measurement error and calibration uncertainty. The revised age ranges sourced from our age-depth modeling also include depth and sedimentation rate uncertainty. For these reasons, the 2σ age ranges from the previous study and those from our study are not directly comparable. We therefore also report the 1σ ranges below.

Charred material associated with scoria fall are likely to be biased towards older ages, which is the case here since the previously-reported ages are older than the stratigraphically-lower Kg tephra (3149 ± 12 cal BP; Tani et al., 2013). We therefore propose revising the ages of the Osawa and Omuro eruptions to 3042 (2965–3085 1σ) and 2930 (2859–3003 1σ) cal BP, respectively, the median values obtained from our age model. This suggests a shorter duration between the two eruptions of ~100 years. The revised age of the Omuro eruption coincides with a large-scale collapse event of unknown origin on the eastern slope (Miyaji et al., 2004), suggesting the latter may be related to simultaneous volcanic activity from other craters of the Fuji volcano. The reworked scoria layer above the Omura fall-layer was deposited ~20 years following the eruptions.

Correlation of the upper three scoria-fall deposits (2,458, 2,438, and 2309 cal BP) is less certain due to the number of eruptions that occurred since deposition of the Kg tephra. The SYP3 and SYP4 pyroclastic density currents appear to have been produced several hundred years prior, and there was a much longer duration between those two eruptions. There are four relatively large eruptions potentially consistent in age with the two scoria layers, the S-20, S-18, S-17, and S-17'. Of these only the S-18 has been dated (2356–2545 cal BP), but none of these have been reported in this area. Following the Kengamine eruption, the last summit eruption (also known as the Yufune; 2328–2122 cal BP; Yamamoto et al., 2011), several small-scale northwestern flank eruptions occurred. However, the ages of these are not well constrained, and the distributions of ejecta are very limited, typically less than 1 km from the craters (Ishizuka et al., 2007; Suzuki et al., 2007). Therefore, it is unlikely that these flank eruptions deposited material in Lake Motosu.

Thus, the age of the youngest scoria-fall layer observed in Lake Motosu, 2309 cal BP (21742452 1σ), is most consistent with the

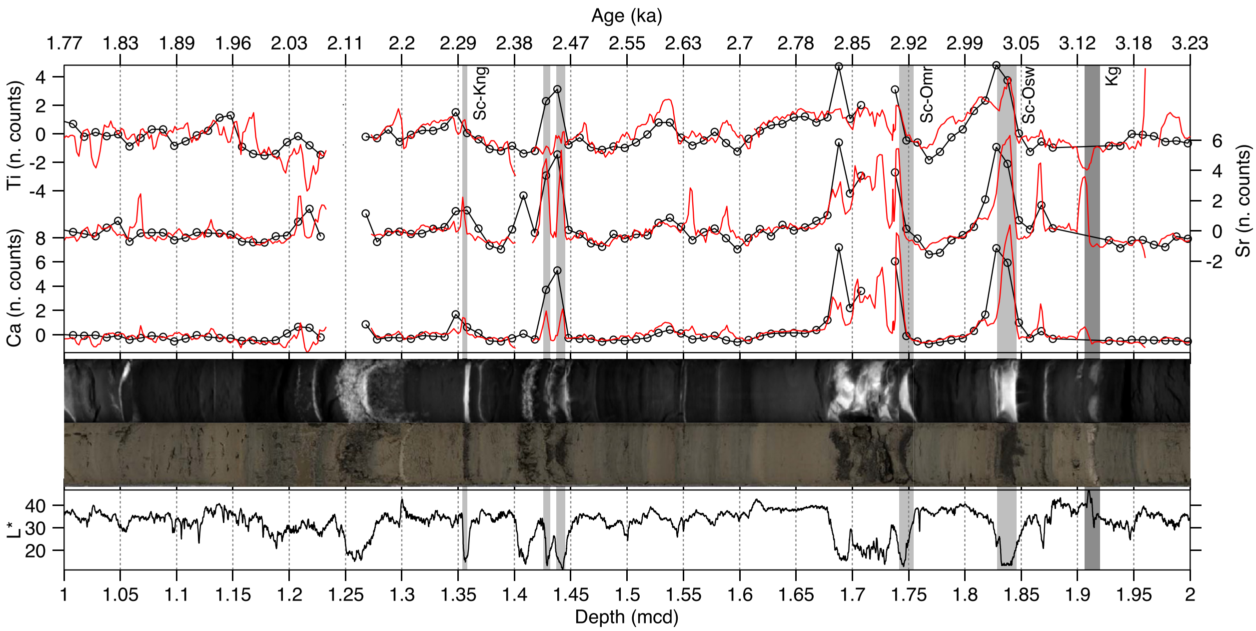

Fig. 11. Shown from bottom to top are Site MOT15-2 L*, composite core image, composite CT image, and scanning XRF data normalized to zero mean and one standard deviation (2-mm Aavatech along Belgian splice: red; 1-cm ITRAX along Japanese splice: black with data-point markers and). Light gray shading indicates scoria-fall layers interpreted to be derived from Mt. Fuji. Dark gray shading indicates the Kg pumice. Based on age, stratigraphic order, and previously reported distributions (Fig. 10), these are interpreted to be the Osawa (Sc-Osw), the Omuro (Sc-Omr), and the Kengamine (Sc-Kng) eruptions. Two additional scoria-fall deposits are detected in Lake Motosu with no clear, corresponding eruption events. (For interpretation of the references to color in this figure legend, the reader is referred to the Web version of this article.)

Kengamine eruption. The two antecedent unknown eruptions preserved in Lake Motosu are older than dates obtained from the Kengamine scoria-associated charred materials. As discussed above, these are typically biased to older ages, and we would therefore expect the ages obtained from the continuously-accumulating lacustrine sequence to produce younger, not older, ages. It appears that the ejecta from the Osawa, Omuro, and Kengamine eruptions is more widely distributed than previously thought.

The remaining two scoria-fall layers identified at 2458 (2331–2590 1σ) and 2438 (2309–2569 1σ) cal BP have no clear corresponding eruptions with similar age ranges, and it is difficult to determine the origin of these two deposits. They could correspond to previously reported eruptions or represent eruptions undetected until now. The short duration between these two distinct events may be insufficient for significant soil development. Thus, on land, they could appear as a single fall-scoria layer, which would have implications for estimating eruption magnitude.

In addition to the possibility of two undetected eruptions, the results presented here provide more accurate ages and indicate a wider distribution of ejecta for the Osawa, Omuro, and Kengamine eruptions during the Subashi-C Stage. Because the distribution of ejecta from previous eruptions indicates the possible affected area during future eruptions, a wider evacuation area should be designated, particularly in the case of eruptions similar to Osawa, Omuro and Kengamine. The more accurate ages reported here, and the implications for eruption frequency, will modify long-term prediction. Thus, these results are relevant to the disaster mitigation plan in the proximity of Mt. Fuji.

6. Conclusions

Lakes proximal to volcanoes are powerful tools for comprehensive reconstruction of eruption history. Lacustrine sediments, even when no annual laminations are present, provide a more accurate and precise means of identifying and dating volcanic sediments than traditional land-based surveys, particularly due to steady recording of inter-event time by background sedimentation processes. A robust chronology, anchored by independently dated tephra layers and terrigenous macrofossils, is constructed through high-density radiocarbon dating. The 8000-year record presented here, from a densely populated region with a large number of annual visitors, reveals potentially previously-undetected Mt. Fuji eruptions, indicates wider distribution of ejecta, and refines the timing of known eruptions. The lacustrine setting allows for clear differentiation of closely spaced events that could otherwise appear as a single larger-magnitude eruption, with implications for estimating the magnitude of past eruptions, long-term prediction, and mitigation planning.

Acknowledgements

This work is part of the "QuakeRecNankai" project, funded by the Belgian Science Policy Office. Additional funding by JSPS Kakenhi 16K05571, 17H01168, and 15KK0151, as well as the University of Tokyo Atmosphere and Ocean Research Institute program for visiting researchers. We thank Takeshi Nakagawa for discussion of operational strategy and M. Murayama for assistance with XRF scanning. Water samples were provided by Air and Water Preservation Division of Yamanashi Prefecture. A portion of this research used data acquired at the XRF Core Scanner Lab at the MARUM — Center for Marine Environmental Sciences, University of Bremen, Germany. Data associated with this study are archived at the Pangaea Data Archive https://doi.pangaea.de/10.1594/PANGAEA.893286.

Appendix A. Supplementary data

Supplementary data related to this article can be found at https://doi.org/10.1016/j.quascirev.2018.09.001.

References

Bertrand, S., Daga, R., Bedert, R., Fontijn, K., 2014. Deposition of the 2011–2012 Cordón Caulle tephra (Chile, 40°S) in lake sediments: implications for tephrochronology and volcanology. J. Geophys. Res.: Earth Surface 119, 2555–2573. https://doi.org/10.1002/2014JF003321.

Blaauw, M., Christen, J.A., Bennett, K.D., Reimer, P.J., 2018. Double the dates and go for Bayes — impacts of model choice, dating density and quality on chronologies. Quat. Sci. Rev. 188, 58–66. http://www.sciencedirect.com/science/article/pii/S0277379118301070.

Blaauw, M., van Geel, B., Kristen, I., Plessen, B., Lyaruu, A., Engstrom, D.R., van der Plicht, J., Verschuren, D., 2011. High-resolution 14C dating of a 25,000-year lake-sediment record from equatorial East Africa. Quat. Sci. Rev. 30, 3043–3059. http://www.sciencedirect.com/science/article/pii/S0277379111002186.

Björck, S., Rittenour, T., Rosén, P., França, Z., Möller, P., Snowball, I., Wastegård, S., Bennike, O., Kromer, B., 2006. A Holocene lacustrine record in the central North Atlantic: proxies for volcanic activity, short-term NAO mode variability, and long-term precipitation changes. Quat. Sci. Rev. 25 (1), 9–32. https://doi.org/10.1016/j.quascirev.2005.08.008.

Fuji Hazard Map Committee Members, 2004. Mt. Fuji Hazard Map Committee Report. Cabinet Office, Government of Japan [Japanese]. http://www.bousai.go.jp/kazan/fujisan-kyougikai/report/.

Fujiwara, O., Machida, H., Shiochi, J.-i., 2010. Tsunami Deposit from the 7,300 Cal BP Akahoya Eruption Preserved in the Yokoo Midden, North Kyushu, West Japan. The Quaternary Research(Daiyonki-kenkyu) 23–33 [Japanese]. https://ci.nii.ac.jp/naid/130004509758/en.

Geospatial Information Authority of Japan, 2018. Ministry of Land, Infrastructure, Transport and Tourism [Japanese]. http://www.gsi.go.jp/kankyochiri/koshouchousa-list.html.

Hamada, H., Katshumata, D., Oyagi, H., 2012. Investigation of Seasonal Change of Water Temperature and Water Quality and Water Balance on Lake Motosu-ko: Bulletin of the Faculty of Education, 66. Chiba University, pp. 459–468 [Japanese with English abstract]. http://opac.ll.chiba-u.jp/da/curator/900116225/.

Ishizuka, Y., Takada, A., Suzuki, Y., Kobayashi, M., Nakano, S., 2007. Eruption ages and whole-rock chemistries of scoria cones on the northern to western slope of Fuji Volcano based on trenching surveys. Bull. Geol. Surv. Jpn. 57, 357–376 [Japanese with English abstract]. https://doi.org/10.9795/bullgsj.57.357.

Koshimizu, S., Uchiyama, T., Yamamoto, G., 2007. Volcanic history of Mt. Fuji recorded in borehole cores from Fuji Five Lakes surrounding Mt. Fuji. In: Aramaki, S., Fujii, T., Nakada, S., Miyaji, N. (Eds.), Fuji Volcano. Yamanashi Institute of Environmental Sciences, pp. 365–374 [Japanese with English abstract].

Lamair, L., Hubert-Ferrari, A., Yamamoto, S., El Ouahabi, M., Vander Auwera, J., Obrochta, S., Boes, E., Nakamura, A., Fujiwara, O., Shishikura, M., Schmidt, S., Siani, G., Miyairi, Y., Yokoyama, Y., De Batist, M., Heyvaert, V.M.A., 2018. Volcanic influence of Mt. Fuji on the watershed of Lake Motosu and its impact on the lacustrine sedimentary record. Sediment. Geol. 363, 200–220. http://www.sciencedirect.com/science/article/pii/S0037073817302610.

Lougheed, B.C., Obrochta, S.P., 2016. MatCal: open source bayesian ^{14}C age calibration in MatLab. J. Open Res. Software 4. http://doi.org/10.5334/jors.130.

Lougheed, B.C., Obrochta, S.P., Lenz, C., Mellström, A., Metcalfe, B., Muscheler, R., Reinholdsson, M., Snowball, I., Zillén, L., 2017. Bulk sediment 14C dating in an estuarine environment — how accurate can it be? Paleoceanography 32, 1944–9186. https://doi.org/10.1002/2016PA002960.

Lougheed, B.C. and Obrochta, S.P., submitted, A Rapid, Deterministic Age-depth Modelling Routine for Geological Sequences with Inherent Depth Uncertainty: Paleoceanography and Paleoclimatology.

Machida, H., 1977. Kazanbai Wa Kataru (Volcanic Ash Is Telling). Soju Shobo, 249 pp. [Japanese].

Machida, H., Arai, F., 2003. Atlas of Tephra in and Around Japan: Tokyo. University of Tokyo Press, 336 pp. [Japanese].

McLean, D., Albert, P.G., Nakagawa, T., Suzuki, T., Staff, R.A., Yamada, K., Kitaba, I., Haraguchi, T., Kitagawa, J., Smith, V.C., 2018. Integrating the Holocene Tephrostratigraphy for East Asia Using a High-resolution Cryptotephra Study from Lake Suigetsu (SG14 Core), Central Japan. Quaternary Science Reviews 18336–58. http://www.sciencedirect.com/science/article/pii/S0277379117306789.

Miyaji, N., 1988. History of younger Fuji volcano. J. Geol. Soc. Jpn. 94, 433–452 [Japanese with English abstract]. https://doi.org/10.5575/geosoc.94.433.

Miyaji, N., Togashi, S., Chiba, T., 2004. A large-scale collapse event at the eastern slope of Fuji volcano about 2900 Years ago. Bull. Volcanol. Soc. Jpn. 49, 237–248 [Japanese with English abstract]. https://doi.org/10.18940/kazan.49.5_237.

Miyairi, Y., Yoshida, K., Miyazaki, Y., Matsuzaki, H., Kaneoka, I., 2004. Improved 14C dating of a tephra layer (AT tephra, Japan) using AMS on selected organic fractions. In: Nuclear Instruments and Methods in Physics Research Section B: Beam Interactions with Materials and Atoms 223 Proceedings of the Ninth International Conference on Accelerator Mass Spectrometry, pp. 555–559. http://www.sciencedirect.com/science/article/pii/S0168583X04006287.

Nakagawa, T., Gotanda, K., Haraguchi, T., Danhara, T., Yonenobu, H., Brauer, A., Yokoyama, Y., Tada, R., Takemura, K., Staff, R.A., Payne, R., Bronk Ramsey, C., Bryant, C., Brock, F., Schlolaut, G., Marshall, M., Tarasov, P., Lamb, H., 2012. SG06, a fully continuous and varved sediment core from Lake Suigetsu, Japan: stratigraphy and potential for improving the radiocarbon calibration model and understanding of late Quaternary climate changes. Quat. Sci. Rev. 36, 164–176. http://www.sciencedirect.com/science/article/pii/S0277379110004440.

Obrochta, S.P., Andrén, T., Fazeka, S.Z., Lougheed, B.C., Snowball, I., yokoyama, Y., Miyairi, Y., Kondo, R., Kotilainen, A.T., Hyttinen, O., Fehr, A., 2017. The undatables: quantifying uncertainty in a highly expanded Late Glacial - holocene sediment sequence recovered from the deepest Baltic Sea basin - IODP Site M0063. G-cubed 18. https://doi.org/10.1002/2016GC006697.

Obrochta, S.P., Crowley, T.J., Channell, J.E.T., Hodell, D.A., Baker, P.A., Seki, A., Yokoyama, Y., 2014. Climate variability and ice-sheet dynamics during the last three glaciations. Earth Planet Sci. Lett. 406, 198–212. https://doi.org/10.1016/j.epsl.2014.09.004.

Reimer, P.J., Bard, E., Bayliss, A., Beck, J.W., Blackwell, P.G., Ramsey, C.B., Buck, C.E., Cheng, H., Edwards, R.L., Friedrich, M., Grootes, P.M., Guilderson, T.P., Haflidason, H., Hajdas, I., Hatté, C., Heaton, T.J., Hoffmann, D.L., Hogg, A.G., Hughen, K.A., Kaiser, K.F., Kromer, B., Manning, S.W., Niu, M., Reimer, R.W., Richards, D.A., Scott, E.M., Southon, J.R., Staff, R.A., Turney, C.S.M., Plicht, J.V.D., 2013. IntCal13 and Marine13 radiocarbon age calibration curves 0–50,000 years cal BP. Radiocarbon 55, 1869–1887. https://doi.org/10.2458/azu_js_rc.55.16947.

Smith, V.C., Staff, R.A., Blockley, S.P.E., Bronk Ramsey, C., Nakagawa, T., Mark, D.F., Takemura, K., Danhara, T., 2013. Identification and correlation of visible tephras in the Lake Suigetsu SG06 sedimentary archive, Japan: chronostratigraphic markers for synchronising of east Asian/west Pacific palaeoclimatic records across the last 150 ka. Quat. Sci. Rev. 67, 121–137. http://www.sciencedirect.com/science/article/pii/S0277379113000413.

Sugihara, S., Fukuoka, T., Ookawara, R., 2001. Volcanic eruptions of tenjouzan volcano at Kozushima and Mukaiyama volcano at Niijima, Izu islands. J. Geogr. 100, 94–105. https://doi.org/10.5026/jgeography.110.94.

Suzuki, Y., Takada, A., Ishizuka, T., Kobayashi, M., 2007. Reexamination of the eruptive history of scoria cones on the northwestern foot of Fuji volcano. Bull. Geol. Surv. Jpn. 57, 337–385. https://doi.org/10.9795/bullgsj.57.377.

Suzuki, Y., Yasuda, A., Hokanishi, N., Kaneko, T., Nakada, S., Fujii, T., 2013. Syneruptive deep magma transfer and shallow magma remobilization during the 2011 eruption of Shinmoe-dake, Japan—constraints from melt inclusions and phase equilibria experiments. J. Volcanol. Geoth. Research 257184–204 http://www.sciencedirect.com/science/article/pii/S0377027313000930.

Takada, A., Yamamoto, T., Ishizuka, Y., Nakano, S., 2016. Geological Map of Fuji Volcano (Second Edition) with Explanatory Text: Miscellaneous Map Series, 12, p. 56 [Japanese with English abstract]. https://www.gsj.jp/Map/EN/docs/misc_doc/misc_12_2nd.html.

Tani, S., Kitagawa, H., Hong, W., Par, J.H., 2013. Age determination of the Kawagodaira volcanic eruption in Japan by 14C wiggle-matching. Radiocarbon 55, 748–752. https://journals.uair.arizona.edu/index.php/radiocarbon/article/view/16312.

Tsuya, H., 1968. Geology of Volcano Mt. Fuji. Explanatory Text of Geological Map 1: 50,000 Scale: Geological Survey of Japan [Japanese with English abstract].

Van Daele, M., Moernaut, J., Silversmit, G., Schmidt, S., Fontijn, K., Heirman, K., Vandoorne, W., De Clercq, M., Van Acker, J., Wolff, C., Pino, M., Urrutia, R., Roberts, S.J., Vincze, L., De Batist, M., 2014. The 600 yr Eruptive History of Villarrica Volcano (Chile) Revealed by Annually Laminated Lake Sediments, 126. Geological Society of America Bulletin, pp. 481–498. https://doi.org/10.1130/B30798.1.

Webster, J.M., Braga, J.C., Humblet, M., Potts, D.C., Iryu, Y., Yokoyama, Y., Fujita, K., Bourillot, R., Esat, T.M., Fallon, S., Thompson, W.G., Thomas, A.L., Kan, H., McGregor, H.V., Hinestrosa, G., Obrochta, S.P., Lougheed, B.C., 2018. Response of the Great Barrier Reef to sea-level and environmental changes over the past 30,000 years. Nat. Geosci. 11, 426–432. https://doi.org/10.1038/s41561-018-0127-3.

Yamamoto, T., Nakano, S., Takada, A., Kobayashi, M., 2011. New stratigraphy of recent eruption products on the eastern slope of the Mt. Fuji volcano. Bull. Geol. Surv. Jpn. 62, 405–424 [Japanese with English abstract]. https://doi.org/10.9795/bullgsj.62.405.

Yamamoto, T., Takada, A., Ishizuka, Y., Miyaji, N., Tajima, Y., 2005a. Basaltic pyroclastic flows of Fuji volcano, Japan: characteristics of the deposits and their origin. Bull. Volcanol. 67, 622–633. https://doi.org/10.1007/s00445-004-0398-y.

Yamamoto, T., Takada, A., Ishizuka, Y., Nakano, S., 2005b. Chronology of the products of Fuji volcano based on new radiometric carbon ages. Bull. Volcanol. Soc. Jpn. 50, 53–70 [Japanese with English abstract]. https://doi.org/10.18940/kazan.50.2_53.

Yamane, M., Yokoyama, Y., Miyairi, Y., Suga, H., Matsuzaki, H., Dunbar, R.B., Ohkouchi, N., 2014. Compound-specific 14C dating of IODP expedition 318 core U1357A obtained off the wilkes land coast, Antarctica. Radiocarbon 56, 1009–1017. https://journals.uair.arizona.edu/index.php/radiocarbon/article/view/17773.

Yokoyama, Y., Anderson, J.B., Yamane, M., Simkins, L.M., Miyairi, Y., Yamazaki, T., Koizumi, M., Suga, H., Kusahara, K., Prothro, L., Hasumi, H., Southon, J.R., Ohkouchi, N., 2016. Widespread collapse of the ross ice shelf during the late holocene. Proc. Natl. Acad. Sci. Unit. States Am. 113, 2354–2359. http://www.pnas.org/content/113/9/2354.abstract.